Korean J. Chem. Eng., 36(2), 299-304 (2019)
DOI: 10.1007/s11814-019-0223-0

pISSN: 0256-1115
eISSN: 1975-7220

In situ electrochemical and mechanical accelerated stress tests of a gas diffusion layer for proton exchange membrane fuel cells

Dongguk Joo*,, Kookil Han***, Jong Hyun Jang**,†, and Sehkyu Park*,†**

*Department of Chemical Engineering, Kwangwoon University, 20 Kwangwoon-ro, Nowon-gu, Seoul 01897, Korea
**Fuel Cell Research Center, Korea Institute of Science and Technology (KIST),
5 Hwarangno 14-gil, Seongbuk-gu, Seoul 02792, Korea
***Fuel Cell Technology Development Team, Eco Technology Center, Hyundai & Kia Motors,
Yongin-si, Gyeonggi-do 16891, Korea
(*Received 1 August 2018 • accepted 14 November 2018*)

Abstract−This study proposes an *in situ* accelerated stress test of a gas diffusion layer (GDL) at a gas-solution-electrode triple phase boundary to individually examine electrochemical and mechanical GDL aging for the first time. Electrochemical GDL stability during repeated potential jumps and mechanical GDL robustness during inert gas permeation were investigated. A Pt-loaded GDL was used to mimic a GDL in contact with Pt particles at the cathode. It was also used to evaluate GDL degradation during an accelerated stress test. In this study, the GDL that experienced an electrochemical stress of potential jumps up to 1.75 V for 27.8 h exhibited 2.9-fold and 4-fold higher losses in electrochemical surface area and oxygen reduction current, respectively, than did one eroded by Ar permeation at 325 cm^3 min^{-1} for 100 h.

Keywords: Proton Exchange Membrane Fuel Cell, Gas Diffusion Layer, *In situ* Accelerated Stress Test, Electrochemical and Mechanical Degradation

INTRODUCTION

Proton exchange membrane fuel cells (PEMFCs) made up of electrolyte, catalyst layer (CL), GDL, and gas flow field gradually degrade during extended operation, thus worsening their performance [1-7]. Particularly, when a fuel cell electric vehicle repeatedly experiences start-up and shut-down (SUSD) events or fuel starvation, carbon-based components in PEMFC stacks can be corroded, because carbon oxidation is thermodynamically favored at >0.207 V (vs. RHE), and its corrosion rate exponentially grows at >1.000 V (vs. RHE) [8-12]. Specifically, Yi et al. [13] proposed a 'reverse-current decay mechanism' for a PEMFC cathode during a simulated SUSD event, reporting a maximum potential at the cathode of 1.443 V (vs. RHE). Tang et al. [14] studied carbon corrosion at the cathode by switching the gas supplied (H_2↔air) at the anode and observed a great potential jump to 1.75 V at the cathode.

Most studies on degradation of PEMFCs caused by electrochemical processes have focused on CL that contains a catalyst metal and catalyst support [12-15]. However, the aging of other carbon-based components, such as GDLs and bipolar plates, has not been extensively addressed. A GDL can be continuously stressed by reactant flow as well as by rapid change in load, so that its original structure and wettability degrade with operating time [16]. Chen et al. [17] immersed in-house dual-layer GDLs in 0.5 M H_2SO_4 solution under high anodic potentials (i.e., 1.0, 1.2, and 1.4 V vs. SCE) for 96 h and then placed the aged GDLs in single cells to evaluate their performance. They found that a microporous layer (MPL) became thinner when the potential applied to a GDL was increased. They also demonstrated that carbon fibers became thinner when the number of macropores in the carbon paper was increased. Accordingly, a single cell that adopted a degraded GDL at 1.4 V vs. SCE showed a 50% lower fuel cell performance than did one with pristine GDL [17]. Chun et al. [18] fabricated a dummy cell made up of a GDL and a Nafion membrane fed with air at 10 L min^{-1} on the GDL side and with liquid water at 65 °C on the membrane side. The GDL with dry air flow for 14 days and subsequently wet air flow for 14 days exhibited many small pits on its surface, along with about a 0.5 wt% carbon loss and 0.5° decrease in contact angle [18]. On the other hand, Roen et al. [19] reported that a cathode with a Pt catalyst produced more CO_2 than one without Pt under potential cycling between 0 and 1.04 V (vs. RHE) for 72 h, and that the cumulative amount of CO_2 generated by carbon corrosion increases with higher Pt loading. They concluded that Pt could accelerate carbon corrosion, depending on the amount of Pt loaded on the electrode [19].

The method suggested by Chen et al. [17] enabled us to independently examine GDL stability against electrochemical stress without interference from other carbon components (e.g., carbon support in CL) or oxidation. The test conducted by Chun et al. [18] could effectively allow a GDL to be stressed by continuous gas flow. However, these methods required fuel cell tests to estimate the modified properties of the GDL after mechanical stress tests. In addition, they were susceptible to undesired damage in the course of stress test cell dissembling and fuel cell assembling [20,21]. Furthermore,

†To whom correspondence should be addressed.
E-mail: vitalspark@kw.ac.kr, jhjang@kist.re.kr

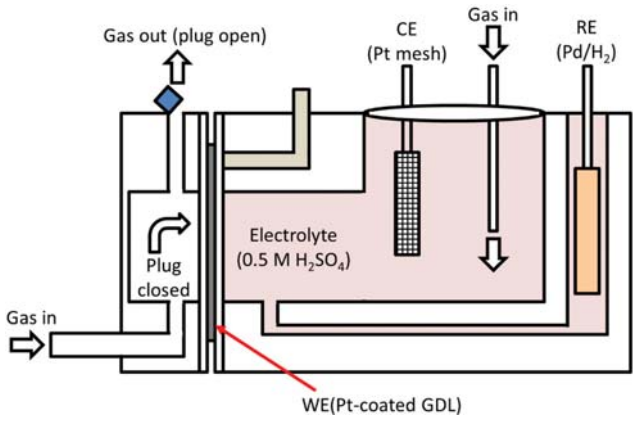

Fig. 1. A schematic of a three-electrode electrochemical cell for electrochemical and mechanical accelerated stress tests of a Pt-coated GDL.

such electrochemical stress for a GDL could not cause carbon corrosion acceleration by Pt catalysts. To discretely examine the electrochemical and mechanical durability of GDLs in the presence of Pt, an *in situ* accelerated stress test (AST) for GDLs is proposed in this study. The effect of electrochemical and mechanical stress on GDL durability was investigated by using a GDL with an unsupported Pt catalyst (i.e., Pt black). Degradation of the GDL is monitored in real time and characterized by different electrochemical and physical methods.

EXPERIMENTAL

Catalyst ink was prepared by ultrasonically blending Pt black (AlfaAesar) with 5 wt% Nafion solution, deionized water, and isopropanol for 20 min. The catalyst ink was applied to carbon paper with MPL (SGL39BC, SGL group) by brushing. The active area was 3 cm^2 and loading of Pt catalyst was 0.3 mg cm^{-2} [22-25]. As shown in Fig. 1, a three-electrode system was constructed using a commercially available electrochemical cell (Gasketal Co., Germany) to make a gas-solution-electrode interface for *in situ* AST. A palladium-hydrogen electrode (Pd/H_2) was employed as the reference electrode to prevent anion adsorption from the reference electrode to the Pt catalyst [26]. Pt mesh was used as the counter electrode, and a GDL loaded with Pt black was used as a working electrode at the gas-solution interface. The Pt catalyst coated on the MPL was in contact with the electrolyte solution.

Electrochemical measurements were carried out using a potentiostat (PGSTAT101, Metrohm Co.). Cyclic voltammetry (CV) was used to measure the electrochemical surface area (ECSA) in Pt during AST. For CV measurements, potential was scanned at 20 mV s^{-1} between 0.05 and 1.05 V (vs. RHE). Ar was introduced to the three-electrode cell at 300 cm^3 min^{-1}. Polarization behavior for the oxygen reduction reaction (ORR) was observed using oxygen at 300 cm^3 min^{-1} to estimate the stability of the GDL loaded with Pt as a function of stressing time. The surface morphology of a GDL with Pt catalyst was observed by means of scanning electron microscopy (Teneo VS™, FEI Co. Ltd.). The surface composition of GDLs was examined using energy-dispersive X-ray spectroscopy (EDS) attached to the SEM.

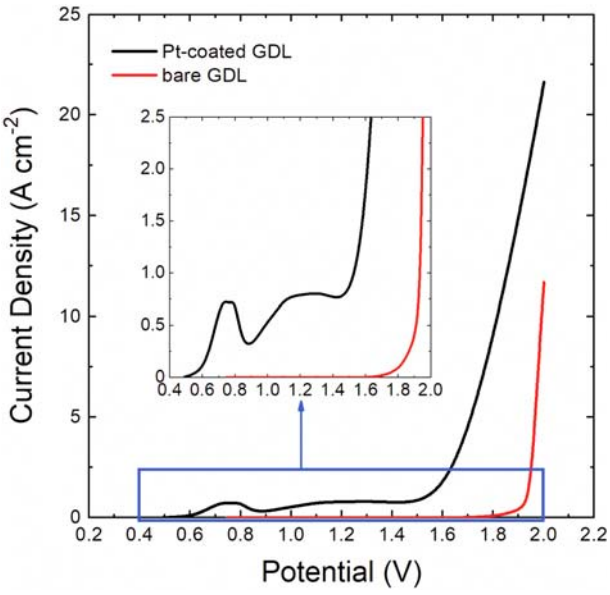

Fig. 2. Linear sweep voltammograms of GDL loaded with Pt and of bare GDL.

RESULTS AND DISCUSSION

Fig. 2 shows polarization behavior of bare GDL and Pt-loaded GDL in the three-electrode electrochemical cell filled with 0.5 M H_2SO_4 in the absence of dissolved O_2. As depicted in Fig. 2, a Pt-loaded GDL began to show anodic current at 0.5 V vs. RHE and a peak between 0.6 and 0.9 V with increasing potential, which might indicate the formation of adsorbed hydroxide on the surface of the Pt (Pt-OH_{ad}). It then gave a second peak between 0.9 and 1.4 V relevant to the Pt-O layer. Subsequently, the anodic current rapidly increased, mainly because of the oxygen evolution reaction (OER) at higher potentials [27]. However, the bare GDL produced no significant current below 1.65 V. It displayed strong anodic current associated with OER above 1.9 V. Experimental polarization data for GDLs with and without Pt imply that carbon particles in the MPL undergo no considerable oxidation below 1.65 V in the absence of Pt particles, whereas the corrosion of carbon particles in contact with Pt can be exacerbated, presumably because various oxygen species are strongly adsorbed onto the surface of Pt adjacent to carbon particles in the MPL.

To study the effect of electrochemical stress on GDL degradation, AST was conducted using potential step change experiments from an open circuit potential of 0.93 V (recorded when hydrogen as a fuel and air as an oxidant are introduced to a PEMFC) to each anodic potential limit proposed by two research groups. First, with a reverse-current decay mechanism [13], 1.45 V as an upper potential limit was adopted for the AST. Fig. 3(a) presents cyclic voltammograms (CVs) between 0.05 and 1.05 V as a function of the number of potential cycles, which consisted of 0.93 V for 5 s and 1.45 V for 5 s with Ar purge at both the GDL and the electrolyte side to give potential stress (see Fig. 1). As shown in Fig. 2, the hydrogen desorption peak at 0.05-0.4 V was slightly increased, while

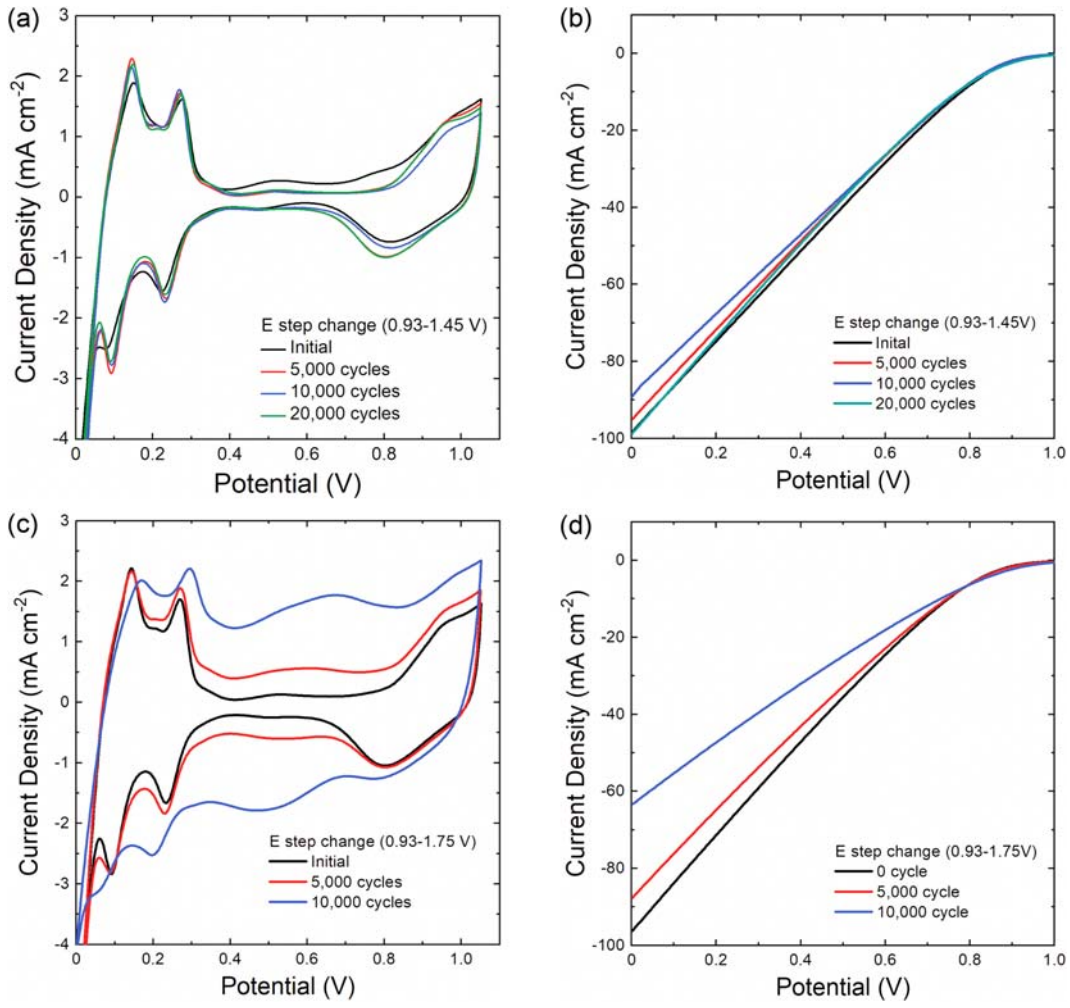

Fig. 3. (a) Cyclic voltammograms of Pt-coated GDL as a function of cycle number. A cycle consists of a potential hold of 0.93 V for 5 s and 1.45 V for 5 s, (b) ORR polarization curves of Pt-coated GDL as a function of cycle number between 0.93 and 1.45 V, (c) cyclic voltammograms of Pt-coated GDL as a function of cycle number. A cycle consists of two potential holds of 0.93 V for 5 s and 1.75 V for 5 s, and (d) ORR polarization curves of Pt-coated GDL as a function of cycle number from 0.93 to 1.75 V.

charging current related to the formation of the electrical double layer during the anodic potential sweep between 0.4 and 0.7 V was decreased after 5,000 potential cycles. However, currents for the hydrogen desorption peak and double layer charging remained almost the same. These results indicate that the ECSA of Pt-loaded GDL is slightly increased, probably because of removal of impurities on the Pt surface without strong adsorption of oxygen species on the Pt and carbon surface. Fig. 3(b) depicts ORR polarization curve of a Pt-loaded GDL with increasing potential cycle from 0.93 to 1.45 V. There was no plateau in the current-potential relationship in Fig. 3(b), although the ORR polarization curve of a diffusion electrode loaded with a catalyst (e.g., a Pt-based catalyst) typically limited the current at low potentials (<0.4 V vs. RHE), because the concentration of oxygen that diffuses to the solution through the GDL (see Fig. 1) is high enough to meet higher ORR current demand without a mass transport limitation. Comparing individual ORR currents in Fig. 3(b) showed that there was no appreciable difference in ORR current regardless of the number of potential cycles. Hence oxygen reduction kinetics at the interface between Pt particles and the solution is still fast under electrochemical stress in the given potential window. Based on experimental CV and ORR polarization data, we think that rapid and repeated potential step changes between 0.93 and 1.45 V trigger no severe oxidation of carbon materials in the GDL.

Next, a similar electrochemical stress test was conducted for a GDL with a higher upper potential limit of 1.75 V, as reported by Tang et al. [14]. Unlike previous results, a great difference between CVs with increasing potential cycle was clearly observed, as shown in Fig. 3(c). The area of hydrogen adsorption and desorption between 0 and 0.3 V was remarkably decreased with a higher number of potential cycles ranging from 0.93 to 1.75 V. Meanwhile, the charging current during an anodic and cathodic sweep vastly grew, perhaps because of the increase in interfacial area between the electrolyte and the electrode (i.e., the GDL in this study) during the electrochemical stress [28,29], and the formation of various oxygen functional groups on the carbon surface, such as hydroquinone and quinone [30], carboxyl or ester groups, carboxyl or ketone groups [31], or quinoidal carbonyl groups [32] with a higher number of

potential cycles. The change in the hydrogen desorption peak and double-layer charging during potential stress up to 1.75 V indicates that carbon particles in the GDL can react with water as oxygen sources, producing CO_{ad} followed by the formation of carbon dioxide. This carbon particle oxidation to carbon dioxide may detach Pt nanoparticles from the GDL, decaying the total charge for hydrogen desorption coupled with ECSA. In addition, after 10,000 potential cycles, the position and area of two (left and right) hydrogen desorption peaks on Pt(110) and Pt(100) below 0.4 V are noticeably different from those in other CVs [33]; hence Pt may both coalesce and detach because of weak interaction between Pt particles and carbon particles in the GDL affected by higher upper potential limit (i.e., 1.75 V) [34]. Fig. 3(d) shows ORR polarization data during repeated potential step changes between 0.93 and 1.75 V. A maximum current measured around 0 V was in decreasing order of 96.2>87.8>63.4 mA cm^{-2} for Pt-loaded GDLs with the number of potential cycles, showing a tendency for ORR polarization. This agrees well with that of hydrogen desorption charge with potential stress at 0.93-1.75 V, as shown in Fig. 3(c).

To examine GDL failure by mechanical stress, Ar permeation through GDL at a high flow rate in the three-electrode cell was carried out without applying potential. To simulate the actual condition of the GDL in PEMFCs, a fixed gas flow rate of 325 cm^3 min^{-1}, equivalent to the amount of air required at 25 °C and 1 atm under constant stoichiometry of 2 to generate 2 A cm^{-2}, was given to the GDL in the three-electrode cell with the gas plug closed (see Fig. 1). CVs of the GDL with continuous Ar flow are presented in Fig. 4(a). A large decrease was found in the hydrogen adsorption and desorption peaks between 0 and 20 h. There was no considerable difference in voltammetric charges between 20 and 100 h. Similarly, Fig. 4(b) shows a slight difference of ORR kinetics with Ar permeation time through the GDL. These results, shown in Fig. 4(a) and (b), indicate that mechanical stress by flowing gas during PEMFC operation might have a relatively low effect on the aging of a cathode GDL. To compare the effect of electrochemical and mechanical stress on the GDL, a total potential hold time at 1.75 V as the electrochemical stressing time was introduced. Fig. 4(c) shows the normalized ECSA for the GDL of interest with each accelerated stress time. ECSA was calculated from total charge for hydrogen desorption in the CV, assuming 210 mC cm^{-2} for the adsorption

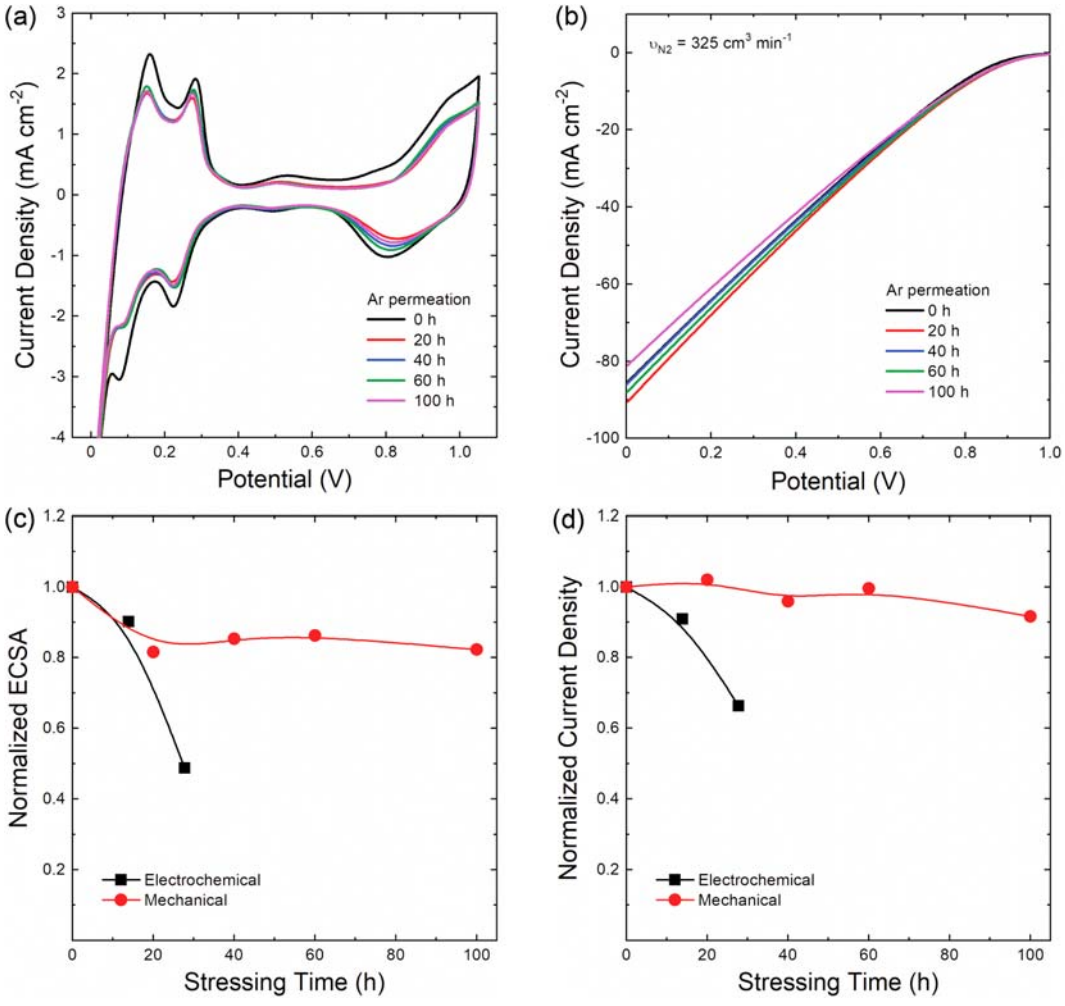

Fig. 4. (a) Cyclic voltammograms of Pt-coated GDL with increasing time of Ar permeation, (b) ORR polarization curves of Pt-coated GDL as a function of Ar permeation time, (c) comparison of normalized ECSA, and (d) normalized ORR current as a function of electrochemical and mechanical stressing time.

of a hydrogen monolayer on Pt. As seen in Fig. 4(c), the electrochemical stress given by repeated potential jumps up to 1.75 V substantially decreased the values of ECSA as the number of potential cycles increased, whereas those calculated from the CVs for mechanical stress remained relatively constant after 20 h. Similarly, the value of current density at 0 V after 100 h of Ar permeation through the GDL was reduced by about 8%. However, the performance loss of the GDL by rapid potential increases from 0.93 to 1.75 V and potential holds at 1.75 V for 13.9 h and 27.8 h were 9.1% and 33.7%, respectively. Comparing electrochemical degradation of the GDL with its mechanical degradation, electrochemical stress between 0.93 and 1.75 V for 27.8 h induced 2.9 and 4.0 times higher ECSA and ORR performance losses, respectively, than did mechanical stress by Ar permeation for 100 h. Experimental data on normalized ECSA and current density with individual stressing times showed that (i) repetitive anodic potential jumped around 1.75 V during SUSD events and fuel starvation relevant to non-uniform fuel distribution at the anode severely impaired the GDL (especially the MPL in contact with Pt particles) as well as the CL compared to the gas flow effect during fuel cell operation, and (ii) the extent of ECSA loss in Pt on the GDL was more severe than that of the decrease in current density connected to the number of triple phase junctions of Pt-ionomer-oxygen during electrochemical stress between 0.93 and 1.75 V.

Fig. 5 displays SEM images of pristine and aged GDLs. The surface of a fresh GDL loaded with Pt black is given in Fig. 5(a). Brush strokes of Pt catalyst ink were clearly found on the GDL with irregularly distributed small holes, but no cracks were seen on the MPL, because they were filled with Pt particles. Surface morphology of an aged GDL caused by 10,000 potential changes at 0.93-1.75 V is presented in Fig. 5(b). Most parts of the MPL were disclosed. Small Pt aggregates were found throughout the MPL, and particularly large Pt aggregates were observed around cracks on the MPL, perhaps because Pt particles are dissolved and detached from the MPL, and Pt particles are redeposited and moved along the surface because of decreased surface energy and then agglomerated during the electrochemical stress [10,35]. A surface image of a mechanically stressed GDL through which Ar was permeated for 100 h is shown in Fig. 5(c). Relatively small Pt aggregates, compared to the specimen shown in Fig. 5(b), were also found on the MPL surface. These were formed during the brushing of Pt catalyst ink that contained ionomer. The coverage of Pt on the surface of the MPL seems to be slightly higher than that on the electrochemically degraded MPL. However, this also shows that fast gas velocity and a long gas path through the GDL can take Pt and carbon particles off and form starfish-like holes.

To qualitatively evaluate Pt loss after individual ASTs, EDS analysis was carried out. Average Pt percent in weight of the GDLs was 83.5, 36.6, and 56.1 for pristine GDL, electrochemically degraded GDL, and mechanically aged GDL, respectively. These results for the electrochemical and physical characterizations of GDLs imply that (i) the MPL surface is damaged by both high potential jumps and continuous shear stress during fuel cell operation, (ii) potential stress causes Pt particles to be separated from the MPL surface and coalesce (these may be relevant to carbon oxidation and Pt particle migration), and (iii) mechanical stress badly triggers erosion of the Pt layer and the MPL, which might have been critically oxidized during the repeated SUSD events, resulting in the detachment of Pt particles while enduring reactant gas flow through the GDL under high electronic load induces serious erosion. Furthermore, water removal from CL to the gas flow channel might have accelerated erosion of the MPL.

CONCLUSION

A novel AST that can separately monitor electrochemical and mechanical GDL aging is proposed in this study using a three-electrode cell with a Pt-loaded GDL that provides triple phase junctions (gas-electrode-solution). Linear scanning voltammograms of GDLs with and without Pt particles revealed that more intense carbon oxidation took place in the presence of Pt on the GDL because of interactions between Pt and oxygen species. To study the effect of electrochemical stress on GDL degradation, two different potential step changes at 0.93-1.45 V and 0.93-1.75 V vs. RHE were performed, and CVs and polarization curves of the Pt-loaded GDLs were obtained with an increasing number of potential cycles (square wave voltammetry with 5 s duration at each potential). Potential jumps up to 1.45 V did not significantly influence diffusion layer corrosion, but repeated potential excursion to 1.75 V allowed carbon particles to bind to oxygen species and lowered carbon surface energy, resulting in Pt particle separation and their coalescence. Mechanical stress done by continuous inert gas flow attacked macropores, making them bigger, and swept many Pt particles (about 47% Pt loss after 100 h Ar flow) loaded on the GDL. *In situ* moni-

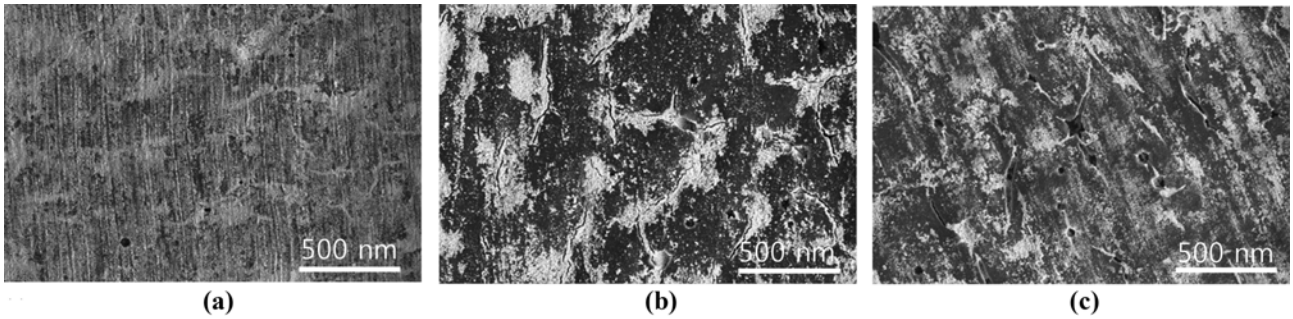

Fig. 5. SEM surface images of (a) pristine Pt-coated GDL, (b) electrochemically degraded Pt-loaded GDL of 10,000 potential cycles between 0.93 and 1.75 V, and (c) mechanically eroded Pt-loaded GDL with Ar permeation for 100 h.

toring of CV and LSV of Pt-loaded GDL during discrete electrochemical and mechanical ASTs offers repeated potential stress (e.g., SUSD events and fuel starvation) that decays ECSA and ORR current by >30% compared to shear stress of the GDL after 27.8 h AST.

ACKNOWLEDGEMENTS

This study was supported by Hyundai Motor Company and by the National Research Foundation of Korea (No. NRF-2016R1D 1A1B03934747), the Korean Government through the National Research Foundation of Korea (No. NRF-2015M1A2A2056554) funded by the MSIT, KIST through the Institutional Programs (No. 2E27301), and Kwangwoon University in 2018.

REFERENCES

1. R. A. Lemons, *J. Power Sources*, **29**, 251 (1990).
2. A. M. Appel, J. E. Bercaw, A. B. Bocarsly, H. Dobbek, D. L. Dubois, M. Dupuis, J. G. Ferry, E. Fujita, R. Hille, J. A. Kenis, C. A. Kerfeld, R. H. Morris, H. F. Peden, A. R. Portis, S. W. Ragsdale, T. B. Rauchfuss, N. H. Reek, L. C. Seefeldt, R. K. Thauer and G. L. Waldrop, *J. Am. Chem. Soc.*, **113**, 6624 (2013).
3. S. Park, Y. Shao, J. Liu and Y. Wang, *Energy Environ. Sci.*, **5**, 9331 (2012).
4. S. Park, Y. Shao, V. V. Viswanathan, J. Liu and Y. Wang, *J. Ind. Eng. Chem.*, **42**, 81 (2016).
5. D. Prasanna and V. Selvaraj, *Korean J. Chem. Eng.*, **33**, 1489 (2016).
6. I.-S. Han, S.-K. Park and C.-B. Chung, *Korean J. Chem. Eng.*, **33**, 3127 (2016).
7. B. Kazeminasab, S. Rowshanzamir and H. Ghadamian, *Korean J. Chem. Eng.*, **34**, 2978 (2017).
8. X. Yuan, H. Li, S. Zhang, J. Martin and H. Wang, *J. Power Sources*, **196**, 9107 (2011).
9. J. Wu, X. Yuan, J. J. Martin, H. Wang, J. Zhang, J. Shen, S. Wu and W. Merida, *J. Power Sources*, **184**, 104 (2008).
10. Y. S. Horn, W. C. Sheng, S. Chen, P. J. Ferreira, E. F. Holby and D. Morgan, *Top. Catal.*, **46**, 285 (2007).
11. X. Yu and S. Ye, *J. Power Sources*, **172**, 145 (2007).
12. S. Yu, X. Li, S. Liu, J. Hao, Z. Shao and B. Yi, *RSC Adv.*, **4**, 3852 (2014).
13. C. A. Reiser, L. Bregoli, T. W. Patterson, J. S. Yi, J. D. Yang, M. L. Perry and T. D. Jarvi, *J. Electrochem. Soc.*, **8**, A273 (2005).
14. H. Tang, Z. Qi, M. Ramani and J. F. Elter, *J. Power Sources*, **158**, 1306 (2006).
15. F. Jia, F. Liu, L. Guo and H. Liu, *Int. J. Hydrogen Energy*, **41**, 6469 (2016).
16. Y. Yamashita, S. Itami, J. Takano, K. Kakinuma, H. Uchida, M. Watanabe, A. Iiyama and M. Uchida, *J. Electrochem. Soc.*, **164**, F181 (2017).
17. G. Chen, H. Zhang, H. Ma and H. Zhong, *Int. J. Hydrogen Energy*, **34**, 8185 (2009).
18. L. M. Roen, C. H. Paik and T. D. Jarvi, *J. Electrochem. Soc.*, **7**, A19 (2004).
19. I. Nitta, T. Hottinen, O. Himanen and M. Mikkola, *J. Power Sources*, **171**, 26 (2007).
20. W. R. Chang, J. J. Hwang, F. B. Weng and S. H. Chan, *J. Power Sources*, **166**, 149 (2007).
21. J. Chun, D. Jo, S. Kim, S. Park, C. Lee and S. Kim, *Renew. Energ.*, **48**, 35 (2012).
22. R. Srivastava, P. Mani, N. Hahn and P. Strasser, *Angew. Chem. Int. Ed.*, **46**, 8988 (2007).
23. E. Daş, S. A Gürsel, L. I. Şanh and A. B. Yurtcan, *Int. J. Hydrogen Energy*, **42**, 19426 (2017).
24. J. Zhao, S. Shahgaldi, I. Alaefour, Q. Xu and X. Li, *Appl. Energy*, **209**, 203 (2018).
25. H. Ishikawa, Y. Sugawara, G. Inoue and M. Kawase, *J. Power Sources*, **374**, 196 (2018).
26. J. Omura, H. Yano, M. Watanabe and H. Uchida, *Langmuir*, **27**, 6464 (2011).
27. W. Vielstich, Fuel Cells: Modern Processes for the Electrochemical Production of Energy, John Wiley & Sons, New York (1970).
28. A. J. Bard and L. R. Faulkner, Electrochemical methods, John Wiley & Sons, New York (1980).
29. S. Park, Y. Shao, H. Wan, V. V. Viswanathan, S. A. Towne, P. C. Rieke, J. Liu and Y. Wang, *J. Phys. Chem. C*, **115**, 22633 (2011).
30. H. Wang, R. Côté, G. Faubert, D. Guay and J. P. Dodelet, *J. Phys. Chem. B*, **103**, 2042 (1999).
31. Z. R. Yue, W. Jiang, L. Wang, S. D. Gardner and C. U. Pittman Jr., *Carbon*, **37**, 1785 (1999).
32. J. Gulyás, E. Földes, A. Lázár and B. Pukánszky, *Compos. Part A-Appl. S.*, **32**, 353 (2001).
33. W. Sheng, Z. Zhuang, M. Gao, J. Zheng, J. G. Chen and Y. Yan, *Nat. Commun.*, **6**, 5848 (2015).
34. Y. Sugawara, T. Okayasu, A. P. Yadav, A. Nishikata and T. Tsuru, *J. Electrochem. Soc.*, **159**, F779 (2012).
35. F. Hasché, M. Oezaslan and P. Strasser, *Phys. Chem. Chem. Phys.*, **12**, 15251 (2010).